Phonon-mediated quasiparticle poisoning of superconducting microwave resonators

U. Patel, Ivan V. Pechenezhskiy, B. L. T. Plourde, M. G. Vavilov, and R. McDermott

Phys. Rev. B **96**, 220501 — Published 7 December 2017

DOI: 10.1103/PhysRevB.96.220501

Phonon-Mediated Quasiparticle Poisoning of Superconducting Microwave Resonators

U. Patel,[1,*] Ivan V. Pechenezhskiy,[1] B. L. T. Plourde,[2] M. G. Vavilov,[1] and R. McDermott[1,†]

[1] *Department of Physics, University of Wisconsin-Madison, Madison, Wisconsin 53706, USA*
[2] *Department of Physics, Syracuse University, Syracuse, New York 13244, USA*

(Dated: November 22, 2017)

Nonequilibrium quasiparticles represent a significant source of decoherence in superconducting quantum circuits. Here we investigate the mechanism of quasiparticle poisoning in devices subjected to local quasiparticle injection. We find that quasiparticle poisoning is dominated by the propagation of pair-breaking phonons across the chip. We characterize the energy dependence of the timescale for quasiparticle poisoning. Finally, we observe that incorporation of extensive normal metal quasiparticle traps leads to a more than order-of-magnitude reduction in quasiparticle loss for a given injected quasiparticle power.

Gate and measurement fidelities of superconducting qubits have reached the threshold for fault-tolerant operations [1, 2]; however, continued progress in the field will require improvements in coherence and the development of scalable approaches to multiqubit control. Recently it was shown that nonequilibium quasiparticles (QPs) represent a dominant source of qubit decoherence [3, 4]. QPs are also a source of decoherence in topologically protected Majorana qubits [5]. Most commonly, superconducting quantum circuits are operated in such a way that there is no explicit dissipation of power on the chip; nevertheless, stray infrared light from higher temperature stages leads to a dilute background of nonequilibrium QPs in the superconducting thin films. According to [6], the leading mechanism for QP relaxation at low density $x = n_{\rm QP}/n_{\rm CP} \lesssim x_* \simeq 10^{-4}$ is trapping by localized defects or vortices, where $n_{\rm QP}$ is the QP density and $n_{\rm CP}$ is the density of Cooper pairs ($4 \times 10^6\ \mu{\rm m}^{-3}$ in Al). In this regime, QPs propagate diffusively through the superconductor until they are trapped.

For future multiqubit processors, however, it might be necessary to integrate proximal control or measurement elements tightly with the quantum circuit, leading to a nonnegligible level of local dissipation. For example, one approach to scalable qubit control involves manipulation of qubits by quantized pulses derived from the classical Single Flux Quantum (SFQ) digital logic family [8, 9]; here, generation of QPs during each voltage pulse is inevitable. Due to the local nature of dissipation, the QP density may become large, $x \gtrsim x_*$, and QP recombination accompanied by phonon emission emerges as the leading mechanism of QP relaxation. The emitted phonons can travel great distances through the substrate until they are absorbed by the superconductor, leading to the generation of new QP pairs [10, 11].

In this manuscript, we present experiments to characterize the dynamics of QP poisoning in superconducting thin films subjected to direct QP injection, so that recombination dominates over trapping at the injection site. We show that cuts in the superconducting film, which eliminate direct diffusion of QPs, have little influence on QP poisoning; however, the incorporation of normal metal QP traps leads to a suppression of QP poisoning by more than an order of magnitude. The data are well explained by a model where injected QPs recombine, emitting high-energy phonons that break pairs in distant parts of the chip. Previous studies from the normal metal-insulator-superconductor (NIS) cooler community have examined the efficiency with which normal metal traps promote removal of nonequilibrium QPs from a superconductor [12–15]. There have been prior attempts to suppress QP poisoning using trapped magnetic flux vortices [16, 17]; however, it can be challenging to trap a large number of vortices controllably while avoiding the associated microwave loss [19]. Recently it was shown that incorporation of normal metal traps that are tunnel-coupled to the superconductor can enhance the QP removal rate by approximately a factor of 4 [6].

In the experiments, we probe QP-induced loss in Al coplanar waveguide (CPW) resonator chips subjected to QP injection via NIS junctions. Schematic cross-sectional views of the devices are shown in Fig. 1a-c. Each die consists of seven $\lambda/4$ CPW resonators capacitively coupled to a common feedline; six NIS junctions are arrayed around the chip perimeter. The device geometry enables investigation of the spatial variation of the instantaneous QP density for a given injection power. The resonators were fabricated from 100 nm-thick Al films grown by sputter deposition on 0.375 mm-thick oxidized Si wafers; the devices were patterned photolithographically and defined with a wet etch. The Cu-AlO_x-Al NIS junctions were next formed in a liftoff process. An ion mill was used to remove the native oxide of the Al prior to controlled oxidation of the tunnel barrier, and the Cu counterelectrode was deposited by electron beam evaporation. The junction areas were $10\,\mu{\rm m}^2$ with specific resistances of order $1.5\,{\rm k}\Omega \cdot \mu{\rm m}^2$. In Fig. 1d we show the micrograph of an injector junction, and in Fig. 1e we show a typical junction $I-V$ curve. We have investigated three geometries:

- *Geometry a* (Figs. 1a, 2a): QPs are injected directly into the groundplane of the chip, and no steps are taken to mitigate QP diffusion or to trap QPs.

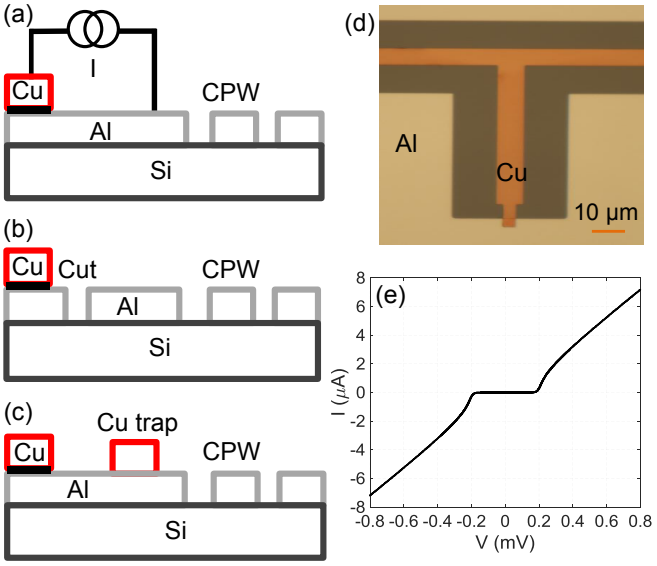

FIG. 1. Schematic cross-sectional view of CPW resonators with NIS injectors for the three geometries studied: (a) direct injection into the groundplane, (b) groundplane cuts around the NIS injector, and (c) coverage of groundplane with normal metal QP traps. (d) Micrograph of the NIS injector. (e) Typical $I-V$ curve of the NIS injector.

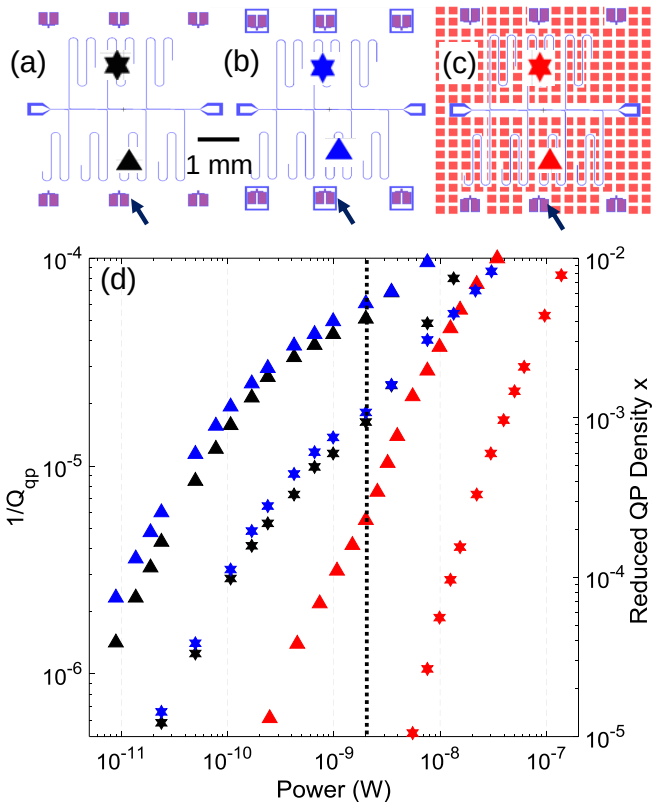

FIG. 2. Layout of multiplexed $\lambda/4$ CPW resonators with NIS injectors for the three geometries studied: (a) direct injection into the groundplane, (b) groundplane cuts around the NIS injector, and (c) coverage of groundplane with normal metal QP traps. The NIS injectors used in these experiments are indicated by arrows. (d) QP loss $1/Q_{\rm qp}$ and density x *versus* injected QP power for geometries *a*, *b*, and *c* (black, blue, and red symbols, respectively). We plot the loss measured in both nearby (triangles) and distant (stars) resonators. The bias voltage $3\Delta/e$ is indicated by the vertical dashed line.

- *Geometry b* (Figs. 1b, 2b): In these devices, the film into which QPs are injected is isolated galvanically from the groundplane of the resonators by 50 μm-wide cuts. These cuts prevent the diffusion of injected QPs to the measurement region.

- *Geometry c* (Figs. 1c, 2c): These devices incorporate a grid of $200\times200\,\mu$m^2 normal metal QP traps arrayed throughout the groundplane with an areal fill factor of 0.44. The traps are deposited as the last step of device fabrication; an *in situ* ion mill clean of the Al underlayer is performed prior to deposition of the 100 nm-thick Cu traps to ensure good metal-to-metal contact.

Devices are cooled to 100 mK in an adiabatic demagnetization refrigerator and transmission across the resonators is monitored using standard homodyne techniques. We fit the frequency-dependent transmission across the resonator and extract the internal and coupling-limited quality factors of the resonator as a function of QP injection rate. We subtract the baseline internal loss measured in the absence of explicit QP injection in order to determine QP loss $1/Q_{\rm qp}$, which is proportional to QP density [3]. In all cases, the microwave drive power is reduced to the point where the measured QP loss $1/Q_{\rm qp}$ shows negligible sensitivity to small changes in microwave drive power [20]; this power level corresponds to an equilibrium photon occupation in the resonators around 5×10^4.

For each device geometry, we characterize QP loss for two resonators: one resonator close to the injection point ($\sim100\,\mu$m at nearest approach) and a second resonator far from the injector (~3 mm away); the locations of these resonators are marked with triangles and stars, respectively, in Fig. 2. We plot QP loss $1/Q_{\rm qp}$ and reduced QP density x *versus* injected QP power in Fig. 2d. The injector resistances are reasonably well matched (140, 140, and 156 Ω for geometries *a*, *b*, and *c*, respectively), so that a given injected power corresponds to a nearly identical range of injection energies.

For geometry *a* (black symbols), we observe the onset of significant dissipation in the nearby resonator as soon as the NIS injector is biased above the gap edge. For the distant resonator, the onset of QP loss is much more gradual, reflecting a reduction in the efficiency of poisoning for the more distant resonators. For geometry *b* (blue symbols), there is no direct path for QPs to diffuse from

the injection point to the resonators due to the presence of the groundplane cuts. Nevertheless, we observe levels of QP poisoning that are nearly identical to those in geometry *a*. The measured dissipation is clearly dominated by a mechanism other than direct diffusion of QPs. For bias points close to the gap edge, QPs near the injection point recombine via emission of 2Δ phonons; these phonons are capable of propagating through the substrate and breaking pairs at distant parts of the circuit. The density of QPs in the injection region can be roughly estimated as $x_{\rm inj} \simeq I_{\rm inj}/(eDdn_{\rm CP})$, where $I_{\rm inj}$ is the injection current, D is the QP diffusion constant, and d is the thickness of the superconducting film. For typical currents $I_{\rm inj} = 1$ μA just above the gap edge and diffusivity $D = 20$ cm^2/s, we find $x_{\rm inj} \approx 8 \times 10^{-3} \gg x_* \simeq 10^{-4}$ [6], so that recombination dominates over QP trapping at the injection site. The range of injected powers considered here is relevant to operation of an SFQ pulse generator, where a single SFQ junction undergoing phase slips at a rate of 5 GHz will dissipate approximately 1 nW. The fact that poisoning via phonon emission is dominant even at the lowest injection energies, rendering ineffective naive attempts to suppress poisoning by limiting diffusion, is the first key conclusion of this work.

At higher biases, the injected QPs quickly relax to the gap edge, emitting athermal phonons. For bias voltages in the range $\Delta/e < V < 3\Delta/e$, these phonons do not have enough energy to break Cooper pairs; as a result, the fraction of injected power that is converted to pair-breaking phonons decreases as injection energy is increased beyond the gap edge. For bias voltage $V > 3\Delta/e$, however, relaxation of injected QPs to the gap is accompanied by emission of phonons with a broad range of energies extending above 2Δ; some of these phonons are capable of breaking pairs in remote regions of the chip. Indeed, we observe a clear enhancement in the QP loss as the injector bias is increased beyond $3\Delta/e$ (indicated by the vertical dashed line in Fig. 2d).

In the case of geometry *c* (red symbols), we find a more than order-of-magnitude suppression of QP loss for a given injected QP power for both the proximal and distant resonators. QPs that diffuse from the superconducting Al film to the normal metal traps will quickly lose most of their energy to conduction electrons via inelastic scattering [18]. Once QPs relax below the gap edge, they do not have enough energy to reenter the superconductor and hence are trapped. As phonon-mediated poisoning proceeds via multiple scattering events, each accompanied by the generation and recombination/relaxation of QPs, extensive coverage of the groundplane with normal metal will limit the flux of pair-breaking phonons from the injection point to the measurement point. The effectiveness with which extensive normal metal coverage suppresses phonon-mediated QP poisoning is the second key conclusion of this work.

Diffusion- and phonon-mediated poisoning should be

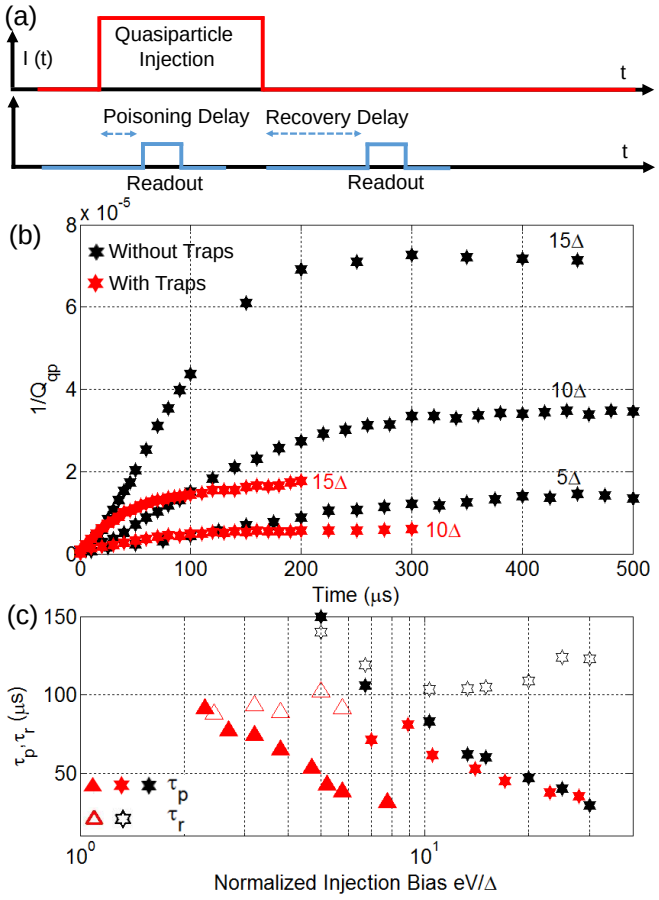

FIG. 3. (a) Pulse sequence for the measurement of QP poisoning and recovery times τ_p and τ_r, respectively. (b) QP loss $1/Q_{\rm qp}$ *versus* time following turn-on of QP injection pulse for devices without (black symbols) and with (red symbols) QP traps. (c) QP poisoning and recovery times τ_p (solid symbols) and τ_r (open symbols), respectively, *versus* normalized injection bias eV/Δ. Triangles correspond to resonators near the injection point, and stars correspond to far resonators (see Fig. 2).

readily differentiated by their dynamics, and we perform additional time-domain experiments to probe the characteristic timescales for QP poisoning and recovery. The experimental pulse sequence is shown in Fig. 3a and the time-dependent QP loss is shown in Fig. 3b. The data reveal that dissipation in the resonator grows monotonically in time, reaching the same values seen earlier in the steady-state measurements. For each device, we fit the data with an exponential function and extract an energy-dependent QP poisoning time τ_p. We find poisoning times of order 100 μs for the lowest injection energies, more than an order of magnitude shorter than the expected time for QP diffusion from the injector to the measurement region. In a related experiment, we monitor QP loss following turn-off of QP injection, and we extract the characteristic QP recovery time τ_r. In Fig.

3c we plot poisoning and recovery times versus bias eV/Δ for geometries a and c (without and with traps, respectively). For both geometries, we find an approximate $1/V$ dependence of the poisoning time. In contrast, there is no apparent voltage dependence for the recovery time. We understand that poisoning depends on the dynamics of phonon generation and propagation via multiple scattering events to the measurement region, as purely ballistic phonon transport would not be affected by the normal traps between the NIS injector and the resonators. On the other hand, recovery is likely dominated by trapping and diffusion of low-energy QPs out of the center trace of the resonators, for which we expect little or no energy dependence.

We use a simple rate equation to analyze the reduced QP density x near the resonators in steady state [17, 23, 24]:

$$r x_i^2(V) + s x_i(V) = g_i(V), \tag{1}$$

where the index $i \in \{\text{near, far}\}$ denotes the location of the resonator; r and s are the QP recombination and trapping rates, respectively; and $g_i(V)$ is the rate of QP generation via pair-breaking phonons. Direct fitting of the experimental data to this equation is complicated by the dependence of the QP generation rate $g_i(V)$ on the bias voltage of the NIS junction. In principle, the QP generation rate $g_i(V)$ could be calculated from the highly athermal phonon distribution in the NIS region and scaled down by a geometry-dependent factor characterizing the efficiency with which pair-breaking phonons propagate from the injector to the measurement region. However, if we assume that the phonon propagation efficiency is energy-independent, we can factor out the bias dependence of the QP generation rate by assuming a fixed ratio between the QP generation rates at the near and far resonator for any given bias V, i.e. $g_{\text{near}}(V)/g_{\text{far}}(V) = \text{const}$. This approach allows us to fit the measured QP densities $x(V)$ with a single voltage-independent value of the ratio r/s. In Fig. 4a we compare the fit to the steady-state QP densities extracted from experiment for the near and far resonators with geometry a (without normal metal traps). From the fit, we find that $r/s \simeq 360$. Using this value of r/s, we extract $g_{\text{near}}(V)/s$ for the near resonator; the result is shown in Fig. 4b.

As discussed above, QPs near the resonators are generated by pair-breaking phonons, and for bias voltage $V < 3\Delta/e$, pair-breaking phonons are only produced by the recombination of QPs near the NIS junction. This picture is supported by the fact that for $V < 3\Delta/e$, the extracted QP generation rate is proportional to the current through the NIS junction, i.e., $g_{\text{near}}(V) \propto \sqrt{(eV/\Delta)^2 - 1}$, as shown in Fig. 4b by the dotted red line. In order to explain the excess QP generation for $V \geq 3\Delta/e$, we have to take into account phonons that are generated by inelastic QP scattering at the NIS junction. These phonons can indeed explain the excess QP

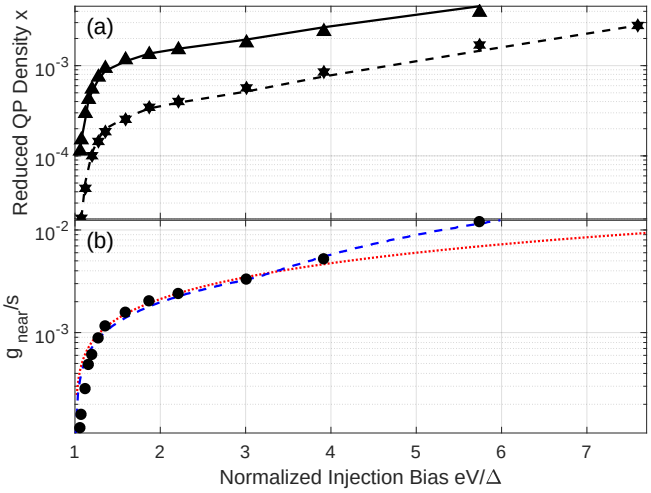

FIG. 4. (a) Steady-state QP density as a function of bias eV/Δ. Triangles and stars are the values extracted from the measured quality factors Q_{qp} and lines are fits to the data. The solid black line and black triangles correspond to the near resonator on sample a (without normal metal traps), while the dashed black line and stars correspond to the far resonator on the same device. (b) Ratio g_{near}/s of QP generation rate to scattering rate for the near resonator of sample a *versus* bias eV/Δ. The black points are extracted from the experimental data; the red dotted line is an appropriately scaled fit to $\sqrt{(eV/\Delta)^2 - 1}$; and the blue dashed line is a fit to a model based on the Boltzmann kinetic equation with energy-dependent QP recombination and scattering rates [3, 21, 22, 25].

poisoning for $V > 3\Delta/e$, as shown in Fig. 4b by the dashed blue line. The latter fit is obtained by scaling the phonon emission rate at the NIS junction calculated from the coupled kinetic equations for the electron-phonon system [3, 21, 22, 25].

The approach of separating the QP dynamics into two separate regions (injection and measurement) is a significant simplification, and a complete model would require proper introduction of a spatial dependence to the QP density [6, 17]. However, the key parameter that justifies our approach and differentiates our work from [6, 17] is the QP density x_{inj} at the injection point. While the QP injection rate in [17] corresponds to an effective current of $0.08\,\mu$A, the injection currents in our measurements span a range from 1-10 μA, corresponding to QP density at the injection site 1-2 orders of magnitude higher. Higher QP density at the injection site enhances QP recombination, which results in the appreciable emission of pair-breaking phonons. In contrast, the data of [6, 17] appear to be in excellent agreement with a model where poisoning proceeds via QP diffusion.

In conclusion, we have performed a systematic study of dissipation due to nonequilibrium QPs in superconducting quantum circuits. We find that the dominant mechanism for QP poisoning is pair breaking mediated by

phonons. We further demonstrate that while diffusion-limiting cuts in the superconducting groundplane are not effective, extensive coverage of the superconducting film with normal metal traps provides a more than order-of-magnitude suppression of QP loss. We anticipate that spatial modulation of the superconducting gap energy to capture QPs in low-gap regions will achieve similar results [27]. Future devices might employ strategies to inhibit the propagation of pair-breaking phonons. For example, engineered discontinuities in the acoustic impedance at the superconductor-substrate interface could inhibit the transmission of phonons into and out of the substrate [28], thus confining them to a small region of the superconducting film that is remote from sensitive quantum devices. These experiments suggest that superconducting quantum circuits can be made robust to modest levels of dissipation on chip, as might be required for the integration of large-scale quantum circuits with proximal classical control and measurement hardware.

We acknowledge stimulating discussions with G. Catelani and L. I. Glazman. This work was supported by the U.S. Government under Grant W911NF-15-1-0248.

* Present address: Argonne National Laboratory, Argonne, Illinois 60439, USA
† Electronic address: rfmcdermott@wisc.edu

[1] A. G. Fowler, M. Mariantoni, J. M. Martinis, and A. N. Cleland, Phys. Rev. A **86**, 032324 (2012).
[2] R. Barends *et al.*, Nature **508**, 500-503 (2014).
[3] J. M. Martinis, M. Ansmann, and J. Aumentado, Phys. Rev. Lett. **103**, 097002 (2009).
[4] G. Catelani, J. Koch, L. Frunzio, R. J. Schoelkopf, M. H. Devoret, and L. I. Glazman, Phys. Rev. Lett. **106**, 077002 (2011).
[5] M. Cheng, R. M. Lutchyn, and S. Das Sarma, Phys. Rev. B **85**, 165124 (2012).
[6] R.-P. Riwar, A. Hosseinkhani, L. D. Burkhart, Y. Y. Gao, R. J. Schoelkopf, L. I. Glazman, and G. Catelani, Phys. Rev. B **94**, 104516 (2016).
[7] R. Barends *et al.*, Appl. Phys. Lett. **99**, 113507 (2011).
[8] R. McDermott and M. G. Vavilov, Phys. Rev. Applied **2**, 014007 (2014).
[9] P. J. Liebermann and F. K. Wilhelm, Phys. Rev. Applied **6**, 024022 (2016).
[10] W. Eisenmenger and A. H. Dayem, Phys. Rev. Lett. **18**, 125 (1967).
[11] O. O. Otelaja, J. B. Hertzberg, M. Aksit, and R. D. Robinson, New J. Phys. **15**, 043018 (2013).
[12] J. N. Ullom, P. A. Fisher, and M. Nahum, Phys. Rev. B **61**, 14839 (2000).
[13] J. P. Pekola, D. V. Anghel, T. I. Suppula, J. K. Suoknuuti, A. J. Manninen, and M. Manninen, Appl. Phys. Lett. **76**, 2782 (2000).
[14] F. Giazotto, T. T. Heikkilä, A. Luukanen, A. M. Savin, and J. P. Pekola, Rev. Mod. Phys. **78**, 217 (2006).
[15] J. T. Muhonen, M. Meschke, and J. P. Pekola, Rep. Prog. Phys. **75**, 046501 (2012).
[16] I. Nsanzineza and B. L. T. Plourde, Phys. Rev. Lett. **113**, 117002 (2014).
[17] C. Wang, Y. Y. Gao, I. M. Pop, U. Vool, C. Axline, T. Brecht, R.W. Heeres, L. Frunzio, M. H. Devoret, G. Catelani, L. I. Glazman, and R. J. Schoelkopf, Nat. Commun. **5**, 5836 (2014).
[18] J. N. Ullom, P. A. Fisher, and M. Nahum, Phys. Rev. B **61**, 14839 (2000).
[19] C. Song, T. W. Heitmann, M. P. DeFeo, K. Yu, R. McDermott, M. Neeley, J. M. Martinis, and B. L. T. Plourde, Phys. Rev. B **79**, 174512 (2009).
[20] P. J. de Visser, D. J. Goldie, P. Diener, S. Withington, J. J. A. Baselmans, and T. M. Klapwijk, Phys. Rev. Lett. **112**, 047004 (2014).
[21] M. Lenander *et al.*, Phys. Rev. B **84**, 024501 (2011).
[22] S. B. Kaplan, C. C. Chi, D. N. Langenberg, J. J. Chang, S. Jafarey, and D. J. Scalapino, Phys. Rev. B **14**, 4854 (1976).
[23] A. Rothwarf and B. N. Taylor, Phys. Rev. Lett. **19**, 27 (1967).
[24] J.-J. Chang and D. J. Scalapino, Phys. Rev. B **15**, 2651 (1977).
[25] For a detailed discussion of the numerical modeling of the coupled QP–phonon system, see Supplemental Material [url], which includes Ref. [26].
[26] G. E. Blonder, M. Tinkham, and T. M. Klapwijk, Phys. Rev. B **25**, 4515 (1982).
[27] J. Aumentado, M. W. Keller, J. M. Martinis, and M. H. Devoret, Phys. Rev. Lett. **92**, 066802 (2004).
[28] S. Kaplan, J. Low. Temp. Phys. **37**, 343-365 (1979).